Ceramics International 45 (2019) 19956–19961

Contents lists available at ScienceDirect

Ceramics International

journal homepage: www.elsevier.com/locate/ceramint

Effects of CNTs content on microstructure and mechanical properties of C_{nt}/α-Al_2O_3 and C_{nt}-C_{sf}/α-Al_2O_3 composites

Jiangang Jia[a,*], Diqiang Liu[a,b], Sheng Zhang[a], Bo Zhang[a], Shunwei Liu[a], Genshun Ji[a]

[a] State Key Laboratory of Advanced Processing and Recycling of Non-ferrous Metals, Lanzhou University of Technology, Lanzhou, 730050, China
[b] School of Materials Science and Engineering, North University of China, Taiyuan, 030051, China

ARTICLE INFO

Keywords:
Alpha-Al_2O_3
Fracture toughness
Flexural strength
CNTs
Short carbon fiber

ABSTRACT

In this work, CNTs and short carbon fiber reinforced α-Al_2O_3 matrix composites (i.e., C_{nt}/α-Al_2O_3 and C_{nt}-C_{sf}/α-Al_2O_3) were prepared by sol-gel dispersing method followed by hot pressing process. Effects of CNTs content on the mechanical properties of C_{nt}/α-Al_2O_3 and C_{nt}-C_{sf}/α-Al_2O_3 composites were investigated and the inter- and transgranular fracture mechanisms in C_{nt}-C_{sf}/α-Al_2O_3 composites were analyzed. The hardness and relative density of C_{nt}/α-Al_2O_3 and C_{nt}-C_{sf}/α-Al_2O_3 composites slightly decrease as CNTs content increases. The flexural strength and fracture toughness monotonically increase with the increase in C_{nt} content for both C_{nt}/α-Al_2O_3 and C_{nt}-C_{sf}/α-Al_2O_3 composites. Addition of C_{sf} and CNTs into α-Al_2O_3 matrix results in a bimodal grain size microstructure of C_{nt}-C_{sf}/α-Al_2O_3 composites, which accounts for the unique fractograph and the enhanced toughness of C_{nt}-C_f/α-Al_2O_3 composites. The flexural strength and fracture toughness of C_{sf}5-nt06 composite are 465 MPa and 7.08 MPa/m^2, 37% and 13% higher than that of C_{nt}06, and 42% and 34% higher than that of C_{sf}5, respectively.

1. Introduction

Alpha-Al_2O_3 is an important structural material with high hardness, high strength, low dielectric dissipation fraction, low thermal conductivity, high elastic modulus, superior wear resistance [1,2]. So far, second phases reinforced Al_2O_3 matrix composites have been widely used as cutting tools, electrical insulators, and dental implants [3]. Of all the second phases, carbon nanotubes (CNTs, below also marked as C_{nt}) and short carbon fiber (marked as C_{sf}) reinforcements are attractive because they have remarkable strength and stiffness, chemical/thermal stability and low density [4–12]. However, when the reinforcement phases are CNTs and/or short carbon fibers, it is often necessary to consider two main factors in the manufacturing process [13]. First, C_{nt} and C_{sf} should not be weakened during the fabrication process. Strength degrading chemical or mechanical attack to C_{nt} and C_{sf} cause weak and brittle behavior of C_{sf}-C_{nt}/ceramic composites. Second, C_{nt} and C_{sf} should be evenly dispersed in the matrices because agglomeration of C_{nt} and/or C_{sf} causes weak bonding between C_{nt} (or C_{sf}) and matrix and therefore restrains the mechanical property improvement of composites [12–15]. Bernal et al. pointed out that the fracture toughness of Al_2O_3-0.1 wt% C_{nt} nanocomposites consolidated by spark plasma sintering (SPS) was reduced by 8%–40% [12]. The degraded fracture toughness ascribed to the agglomeration of C_{nt}. Sarkar et al. reported that the mechanical properties of CNT/Al_2O_3 nanocomposites decreased when the C_{nt} content surpassed 0.3 vol% due to the difficult dispersion of C_{nt} [14]. Obviously, homogeneous dispersion of C_{nt} and C_{sf} is very important to obtain high toughness/strength of Al_2O_3 matrix.

For the purpose of uniformly dispersing C_{nt} or C_{sf} into ceramic matrices, various dispersion techniques have been used to fabricate C_{nt} and C_{sf} reinforced ceramic composites, such as slurry infiltration [16,17], electrophoretic deposition [18], sol-gel, solvent incorporation [5], ultrasonication, and ball milling, etc. [3,19–21]. Among all of the fabrication processes, ball milling is a widely used method to uniformly disperse C_{nt} and C_{sf} into ceramic matrices [4,22]. However, ball-milling method may suffer from damaging the C_{nt} or C_{sf} reinforcements. Sol-gel dispersing is an effective way to uniformly disperse C_{nt} and C_{sf} into Al_2O_3 matrix because viscous gel is able to "capture and fix" C_{nt} and C_{sf} and effectively prevents the agglomeration of C_{nt} or C_{sf} dispersed in it. The defect sites on carbon fiber and CNTs surface contain unbounded electrons and are therefore capable of participating in some form of stable bonding with the -OH and -OOH functional groups and other species in AlOOH gel to immobilize the C_{sf} and C_{nt}.

In our previous investigation [13], we prepared C_{sf}/α-Al_2O_3 composites based on sol-gel dispersing strategy and systematically investigated effects of short carbon content on the mechanical properties of C_{sf}/α-Al_2O_3 composites. Results show that when the short carbon

* Corresponding author.
E-mail address: lzhjiajiangang@163.com (J. Jia).

https://doi.org/10.1016/j.ceramint.2019.06.253
Received 6 May 2019; Received in revised form 20 June 2019; Accepted 24 June 2019
Available online 25 June 2019

fiber content is 5 vol%, the C_{sf}/α-Al_2O_3 composite has the highest bending strength value of 336 MPa. However, the C_{sf}/α-Al_2O_3 composites prepared based on the sol-gel dispersing method have coarse matrix grains, which limit the improvement of strength of the fiber-reinforced composites. In order to inhibit matrix grain growth and further improve composite strength, 0.2–0.6 wt% CNTs were uniformly introduced into 5 vol%-C_{sf}/α-Al_2O_3 composites. The effects of CNTs content on the microstructure and mechanical properties of α-Al_2O_3 matrix and C_{sf}/α-Al_2O_3 composites were systematically investigated.

2. Experiments and characterization

2.1. Materials and processing

In this paper, series of C_{nt}/α-Al_2O_3 composites with different content of C_{nt} (0.2, 0.4, 0.6 wt%) were prepared via sol-gel dispersing method followed by hot pressing at 1500 °C for 1 h. Likewise, C_{nt}-C_{sf}/α-Al_2O_3 composites with 0.2, 0.4, 0.6 wt% C_{nt} were fabricated through the same procedure. Each C_{nt}-C_{sf}/α-Al_2O_3 composite has a fixed C_{sf} content of 5 vol %. For comparison, pristine α-Al_2O_3 and α-Al_2O_3-5vol % C_{sf} were also prepared. The compositions and codes of the as prepared composites listed in Tables 1 and 2.

Multi-walled carbon nanotubes (purity: 99%, diameter: 15–130 nm) were obtained from Shenzheng Nanoport Co., Ltd (Shenzhen, China). PAN based carbon fibers with an average diameter of 7 μm and tensile strength of 2800 MPa were supplied by Gansu Haoshi Carbon Fiber Co., Ltd (Gansu, China). Aluminum isopropoxide ($C_9H_{21}AlO_3$, purity: > 99%) was achieved from Tianjin Guangfu Fine Chemical Research Institute and used to fabricate AlOOH sol-gel. The preparation process of AlOOH sol-gel has been described in literature [23]. Ball milled TiO_2 + CuO powder mixtures (weight ratio: 80 to 20) were used as sintering aids [13]. Multiwalled carbon nanotube and/or chopped carbon fibers (length: 2–3 mm) were added into the boehmite gel and mechanically stirred until the C_{nt} and/or C_{sf} uniformly dispersed. The green part was obtained by compacting the gel mixture (dried at 75 °C for 2 h) under a uni-axial pressure of 40 MPa. Then, the green part was calcinated at 460 °C for 4 h and hot pressed at 1500 °C for 1 h to get the C_{nt}/α-Al_2O_3 and C_{nt}-C_{sf}/α-Al_2O_3 composites. Fig. 1 schematically depicts the fabrication procedure of the C_{nt}/α-Al_2O_3 and C_{nt}-C_{sf}/α-Al_2O_3 composites.

2.2. Characterization methods

Field emission scanning electron microscopy (SEM, FEI MAGELLAN 400, American) was used to observe the fracture surface of the C_{nt}/α-Al_2O_3 and C_{nt}-C_{sf}/α-Al_2O_3 composites. Bulk densities of the samples were gauged according to Archimedes' methods with deionized water. Vickers hardness tester (HV-30, Jinan Fengzhi Test Instrument Co., Ltd., Jinan, China) was employed to measure hardness of the composites. Three-point bending tests were carried out using a universal testing machine (MTS E44.304, American) to assess the flexural strength. The rectangular specimens for three-point bending tests have a dimension of 3 × 4 × 20 mm^3. The span was 16 mm and the crosshead displacement rate was 0.05 mm/min. The flexural strength σ was calculated by the following equation.

Table 1
Compositions and codes for C_{nt}/α-Al_2O_3 composites.

Codes	Content of carbon nanotubes (wt%)	Content of sintering aid (wt%)
$C_{nt}0$	0	2
$C_{nt}02$	0.2	2
$C_{nt}04$	0.4	2
$C_{nt}06$	0.6	2

Table 2
Compositions and codes for C_{nt}-C_{sf}/α-Al_2O_3 composites.

Codes	Content of carbon nanotubes (wt%)	Content of carbon fiber (vol%)	Content of sintering aid (wt%)
$C_{sf}5$	0	5	2
$C_{sf}5$-nt02	0.2	5	2
$C_{sf}5$-nt04	0.4	5	2
$C_{sf}5$-nt06	0.6	5	2

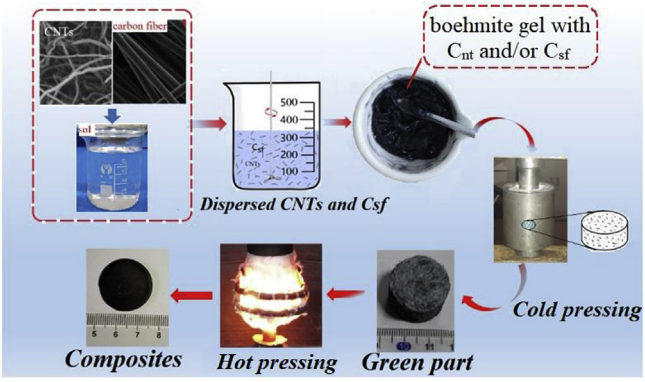

Fig. 1. Schematic diagram of fabrication procedure of the C_{nt}/α-Al_2O_3 and C_{nt}-C_{sf}/α-Al_2O_3 composites.

$$\sigma = \frac{3PL}{2bd^2} \tag{1}$$

where P is the break force, L the outer (support) span, b specimen width, and d the specimen thickness. Single edge notch-beam (SENB) specimens were used to gauge the fracture toughness during three-point-bending test. The SENB samples, which contain a fixed razor-blade notch (0.25 mm) using a 0.2 mm thick diamond blade, have a dimension of 2 mm × 4 mm × 24 mm and a span of 16 mm. At least four specimens were tested under each test condition. The fracture-toughness (K_{IC}) was calculated by employing equation (2) according to ASTM standard E399.

$$K_{IC} = \frac{3PL\sqrt{a^{10^{-3}}}}{2BW^2}\left[1.93 - 3.07\left(\frac{a}{W}\right) + 14.53\left(\frac{a}{W}\right)^2 - 25.07\left(\frac{a}{W}\right)^3\right] + 25.08\left(\frac{a}{W}\right)^4 \tag{2}$$

where P represent peak-load at fracture (N), L the specimen-span (mm), B the specimen-thickness (mm), W the specimen-width (mm) and a correspond to crack-length (mm).

3. Results

3.1. Dispersion of C_{nt} and C_{sf}

Fig. 2 shows the SEM images of short carbon fibers and multi-walled carbon nanotubes used in this study. As shown in Fig. 2a, the diameter of carbon fiber determined by SEM observation is about 7 μm and the surface of carbon fiber is smooth together with fine-integrity. The CNTs with diameters range from 15 nm to 200 nm appear to be extraordinarily curly and entangled with each other (Fig. 2b). The curly nature and entanglement of CNTs imply that it is difficult to evenly disperse them into Al_2O_3 matrix.

Sol-gel dispersion strategy not only allows the short carbon fibers to be uniformly dispersed, as reported in our previous work [13] but also enables CNTs to be randomly distributed into the AlOOH sol-gel. It is noted that the carbon fiber length in the 2- to 10-mm interval has no obvious effects on the mechanical properties of the composites, only increases the "clumping" tendency of the fibers. This is in accordance

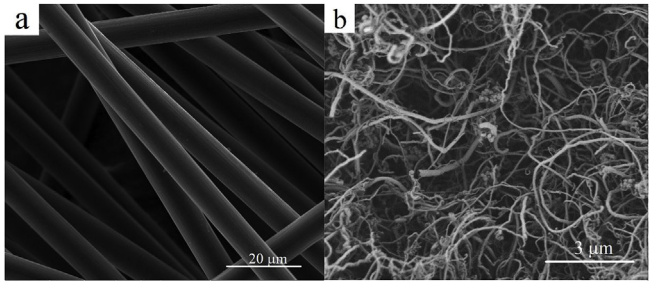

Fig. 2. Scanning electron microscopy micrographs of short carbon fibers (a) and CNTs (b).

with other investigations [4].

Because of large specific surface area of the CNTs, on the one hand, CNTs have high agglomeration clustering tendency, as depicted in Fig. 2b and pointed out in other investigations [24]. On the other hand, when the CNTs are dispersed in AlOOH sol-gel, defect sites on CNTs surface can form some strong bonding like O-OH/C = O and hydrogen bond with the functional groups in the sol-gel. In this later case, strong interactions between CNTs and sol-gel finally result in the uniform distribution of CNTs in AlOOH sol-gel under vigorous mechanical stirring condition (Fig. 3b). It is clear that AlOOH gel containing CNTs do not affect uniform dispersion of short carbon fibers (Fig. 3a).

3.2. Mechanical properties

The hardness and density results of $C_{nt}/\alpha\text{-}Al_2O_3$ and $C_{nt}\text{-}C_{sf}/\alpha\text{-}Al_2O_3$ composites with different CNTs content are listed in Table 3. It is shown that density and relative density of $C_{nt}/\alpha\text{-}Al_2O_3$ and $C_{nt}\text{-}C_{sf}/\alpha\text{-}Al_2O_3$ composites are decreased as the CNTs content increases. The hardness of the $C_{nt}/\alpha\text{-}Al_2O_3$ and $C_{nt}\text{-}C_{sf}/\alpha\text{-}Al_2O_3$ composites is closely related to the relative density and porosity. With relative density decreasing, the hardness of composites slightly decreases. Except for $C_{nt}06$, which has a relative density of 94.72%, the relative density of all samples exceeds 95%, which means that the porosity of the samples prepared in the present work is low. Fig. 4 shows the flexural strength and fracture toughness of $C_{nt}/\alpha\text{-}Al_2O_3$ and $C_{nt}\text{-}C_{sf}/\alpha\text{-}Al_2O_3$ composites. With CNTs content increasing from 0 to 0.6 wt%, flexural strength and fracture toughness of $C_{nt}/\alpha\text{-}Al_2O_3$ increase gradually. All of the $C_{nt}/\alpha\text{-}Al_2O_3$ composites exhibit higher flexural strength and fracture toughness than that of $C_{nt}0$ (viz. monolithic $\alpha\text{-}Al_2O_3$). Flexural strength and fracture toughness of $C_{nt}06$ are 350 MPa and 6.3 MPa/m^2, respectively, which are 115% and 80% higher than that of $C_{nt}0$, respectively. In the case of $C_{nt}\text{-}C_{sf}/\alpha\text{-}Al_2O_3$ composites, mechanical properties also show an increase in flexural strength and fracture toughness as a function of CNTs content. The flexural strength and fracture toughness increase from 336 MPa to 5.2 MPa/m^2 for $C_{sf}5$ to 465 MPa and 7.08 MPa/m^2 for $C_{sf}5$-nt06, respectively. $C_{sf}5$-nt06 composite shows the highest flexural

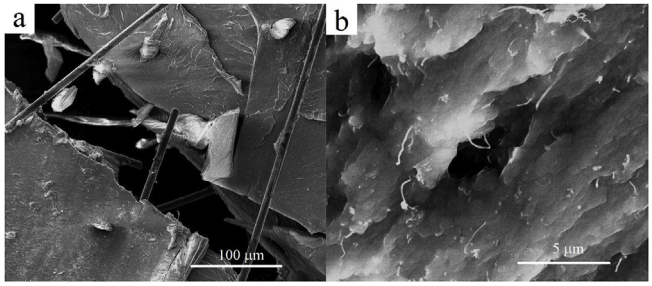

Fig. 3. Short carbon fibers and CNTs dispersed in the AlOOH-gel, (a) low magnification SEM image showing the dispersion of short carbon fibers in AlOOH-gel and (b) higher magnification image showing the uniform distribution of CNTs in AlOOH-gel.

Table 3
Density and hardness of $C_{nt}/\alpha\text{-}Al_2O_3$ and $C_{nt}\text{-}C_{sf}/\alpha\text{-}Al_2O_3$ with different CNTs content.

Samples	Density (g/cm^3)	Relative density (%)	Hardness (HV)
$C_{nt}0$	3.92	98.7	1705
$C_{nt}02$	3.9	98.34	1690
$C_{nt}04$	3.81	96.18	1675
$C_{nt}06$	3.72	95.44	1650
$C_{sf}5$	3.85	98.24	1730
$C_{sf}5$-nt02	3.81	97.32	1629
$C_{sf}5$-nt04	3.76	96.15	1591
$C_{sf}5$-nt06	3.7	94.72	1565

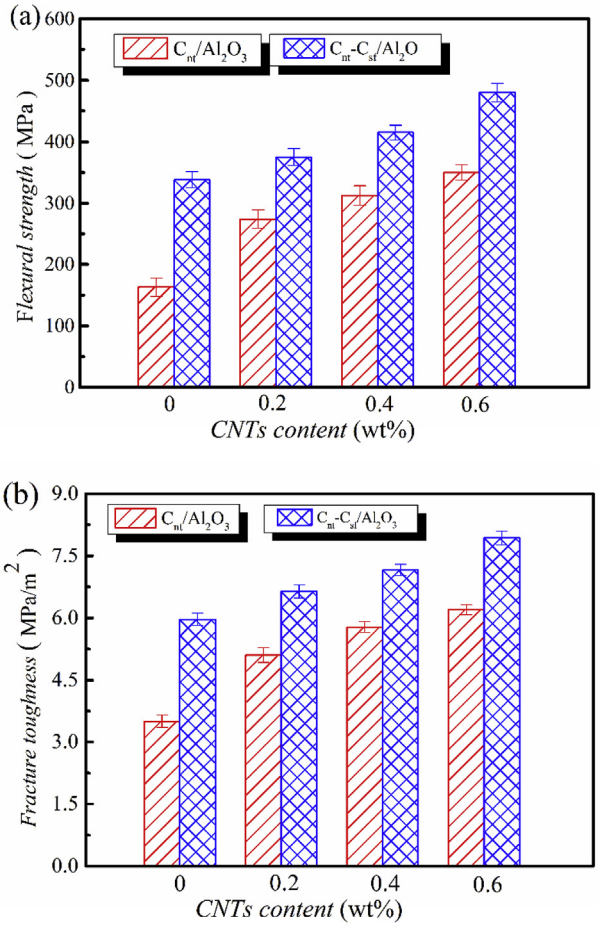

Fig. 4. Mechanical properties of $C_{nt}/\alpha\text{-}Al_2O_3$ and $C_{nt}\text{-}C_{sf}5/\alpha\text{-}Al_2O_3$ composites with different CNTs content, (a) flexural strength (b) fracture toughness.

strength and fracture toughness, which are 185.3% and 102.9% higher than that of $C_{nt}0$, 37% and 13% higher than that of $C_{nt}0.6$, and 42% and 34% higher than that of $C_{sf}5$, respectively. The higher fracture toughness means that the $C_{nt}\text{-}C_f/\alpha\text{-}Al_2O_3$ composites consume more energy during fracture, and that the cracks propagation in $C_{nt}\text{-}C_f/\alpha\text{-}Al_2O_3$ is more stable than that of $C_{nt}/\alpha\text{-}Al_2O_3$ composite [25].

Fig. 5 shows the typical load vs. crosshead displacement curves for $C_{nt}/\alpha\text{-}Al_2O_3$ and $C_{nt}\text{-}C_{sf}/\alpha\text{-}Al_2O_3$ composites. We can see that the maximum values of load and displacement for both $C_{nt}/\alpha\text{-}Al_2O_3$ and $C_{nt}\text{-}C_{sf}/\alpha\text{-}Al_2O_3$ composites increase as CNTs content increases. At the initial stage, the curves show a nonlinear region of different extent and then the applied load increase linearly as the displacement increases. Comparing with $C_{nt}/\alpha\text{-}Al_2O_3$ composites, the maximum load and the displacement to fracture for $C_{nt}\text{-}C_{sf}/\alpha\text{-}Al_2O_3$ are increased. Both larger load and displacement of $C_{nt}\text{-}C_{sf}/\alpha\text{-}Al_2O_3$ result in higher flexural

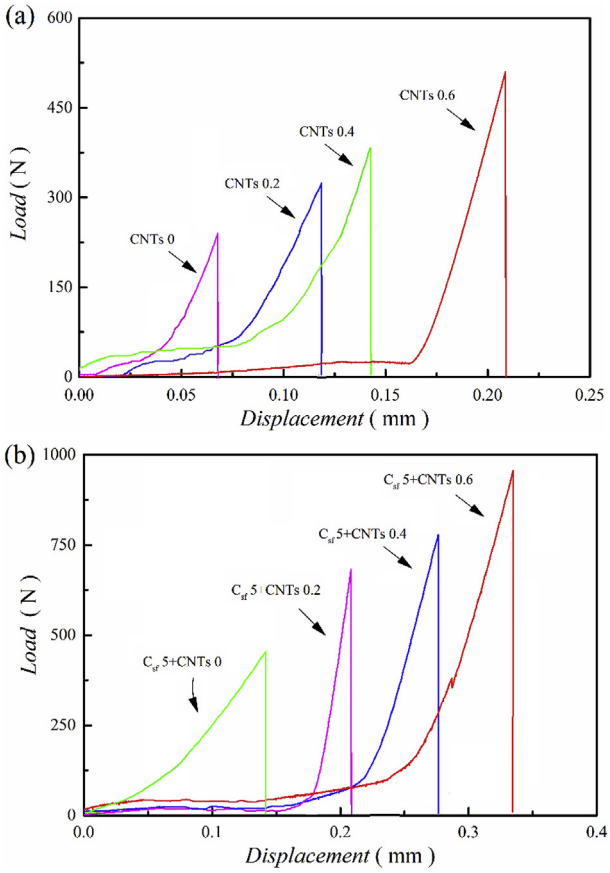

Fig. 5. Typical load-displacement curves of C_{nt}/α-Al_2O_3 composites (a) and C_{nt}-C_{sf}/α-Al_2O_3 composites (b).

strength and fracture toughness, as presented in Figs. 5 and 4, indicating the significant synergistic strengthening and toughening effect from C_{nt} and C_{sf}.

3.3. Morphologies of fracture surfaces

Fig. 6 shows fractography of $C_{sf}5$ and $C_{nt}06$. The grains of $C_{sf}5$ are irregular in shape and the size of the grain is large, accompanied with small amount of finer ones (Fig. 6a). The fracture surface of $C_{nt}06$ demonstrates much finer grains with small amount of distinct intragranular pores, as shown in Fig. 6b. The resulting finer grains of $C_{nt}06$ are due to the effect of C_{nt} inhibiting grain growth. The intragranular pores either are residual porosity as the result of sintering procedure, which are often less detrimental to the compactness and properties of C_{nt}/α-Al_2O_3 composites, or derived from pulling-out of CNTs that can substantially enhance the α-Al_2O_3 matrix.

The microstructure characteristic of C_{nt}-C_{sf}/α-Al_2O_3 composites change markedly compared with the C_{sf}/α-Al_2O_3 composites due to

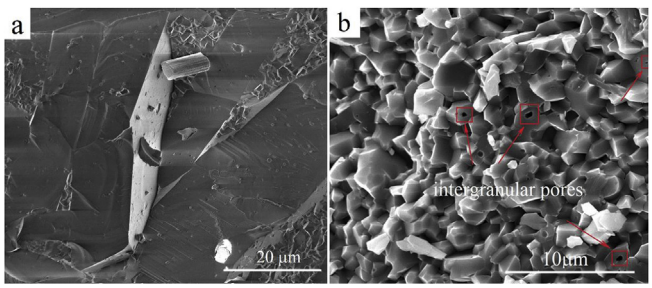

Fig. 6. Fractographs of $C_{sf}5$ (a) and $C_{nt}0.6$ (b).

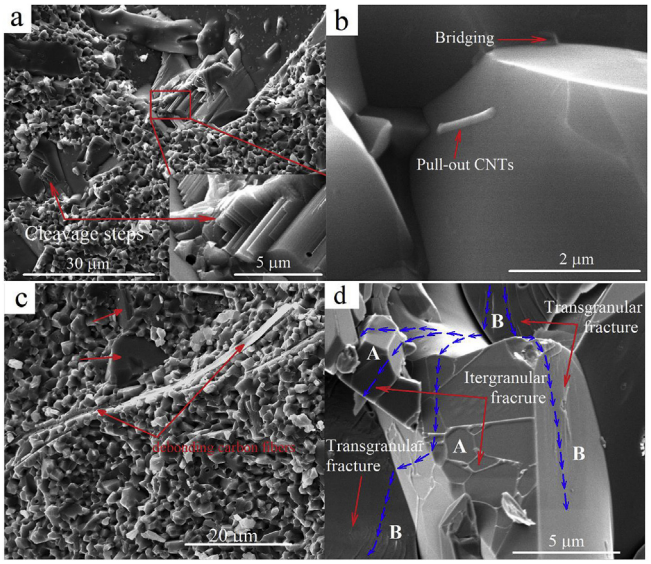

Fig. 7. Fractographs of $C_{sf}5$-nt0.2(a), (b) and $C_{sf}5$-nt0.6 (c), (d).

introduction of CNTs. Bimodal grain size distributions clearly observed by SEM of fracture surface, i.e., a fine grain matrix with random distribution of much larger grains, as shown in Fig. 7a and c. In addition, the larger grain population, as well as their size, decreases as the carbon nanotube content increases, whereas the microstructure of fine grain matrix of C_{sf}-nt06 is similar to $C_{nt}06$ (Fig. 6b). The fracture mode of C_{nt}-C_{sf}/α-Al_2O_3 composites, the average trend over the fracture surface, is for finer grain fracture to be mainly, but not exclusively, intergranular, and for larger grain fracture to be mainly, almost exclusively, transgranular fracture. Carbon nanotube pull-out hole and cleavage steps are observed in the insert of Fig. 7a, and carbon nanotube pullout and bridging are observed in Fig. 7b, which provide substantial evidence of C_{nt} toughness mechanism in C_{nt}-C_{sf}/α-Al_2O_3 composites. Carbon fiber debonding amongst finer grain matrix is observed in Fig. 7c. Both inter- and transgranular fracture can be observed in Fig. 7d. The arbitrary drawn arrow lines demonstrate possible crack propagation paths in the C_{nt}-C_{sf}/α-Al_2O_3 composites. Crack tortuosity and branching clearly occur and generate local complex fracture surface in $C_{sf}5$-nt06.

4. Discussion

Microstructure parameters, which include matrix grain size, shapes, orientations, reinforcements, and the numerical and spatial distributions of these, have a great influence on the mechanical properties and fracture behaviors of a material. The addition of short carbon fibers to α-Al_2O_3 ceramic has shown significant ductile enhancement (and, subsequently, fracture toughness improvement) for α-Al_2O_3 matrix composites in our previous work [13] and other investigations [26,27], owing to crack bridging, crack deflection, fiber pullout, fiber debonding etc., making crack propagation more difficult. In the present work, it is shown that the mechanical properties of C_{nt}/α-Al_2O_3 composites are strongly dependent on the CNTs content and microstructure. CNTs dispersed in α-Al_2O_3 matrix can effectively bear the load applied to composites, and thus promote the increasing of flexural strength and fracture toughness. Introducing different content of CNTs into 5 vol % C_{sf} reinforced α-Al_2O_3 composite monotonically increase the flexural strength and fracture toughness of C_{nt}-C_f/α-Al_2O_3 composites. In addition, inevitable local variation in distribution of the reinforcing phases (C_{sf} and CNTs) and sintering aids are considered to be the major cause of abnormal grain growth. Local variation in the microstructure leads to initial difference in boundary energy or mobility [28]. At the presence of the sintering aids, partial liquid phases can be generated during sintering process [29]. Besides enhancing mass transfer and

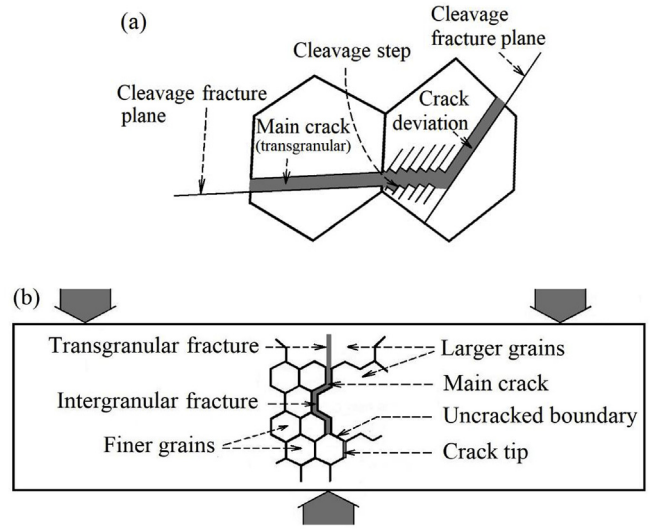

Fig. 8. Schematic of possible crack mechanism of nacre like cleavage step (a) and intergranular fracture (b).

promoting the densification of Al_2O_3 matrix, liquid phases tends to selectively wet the low-energy boundaries and enhance the mobility difference between the non- and wetted boundaries, leading to anisotropic abnormal grain growth because growth is rapid parallel to and slow normal to the wetted, low-energy boundaries [28]. Consequently, bimodal grain size microstructure that accounts for the unique fractograph and the enhanced toughness of C_{nt}-C_f/α-Al_2O_3 composites occurs.

Fig. 8a shows, in a schematic fashion, how the cleavage steps form in a transgranular-fractured grain. Cleavage fracture is the most brittle form of fracture and usually occurs along specific crystallographic planes. For α-Al_2O_3, {1010} and {1012} planes would be the preferred fracture planes because the surface energy of these planes are much lower than that of the basal plane (0001) [30]. When a cleavage crack passes through a grain boundary, the cleavage crack would change its direction because of different orientations of the adjacent grains. In order for the main crack continues to propagate along the previous direction, cleavage steps may form before the main crack deviation occurs. This process substantially reduces energy release rate and renders propagation of a crack more difficult. When the crack encounters finer grain boundaries, fracture crack may enter the grain boundaries and intergranular fracture occurs, as illustrated in Fig. 8b and evidenced in Fig. 7d. The mechanism of intergranular fracture is proposed based on fracturing of grain boundary facets at the crack tip, which are then linked to the main crack via cracking of a previously uncracked boundary [31]. Since stress concentrations are higher over finer boundary facets than those over the larger ones, it is reasonable that finer grain boundaries favor intergranular fracture and large grains tend to undergo transgranular fracture.

5. Conclusion

(1) Sol-gel dispersing method was an effective way to uniformly distribute the C_{nt} and C_{sf} into α-Al_2O_3 matrix. The flexural strength and fracture toughness monotonically increase with the increase in C_{nt} content for both C_{nt}/α-Al_2O_3 and C_{nt}-C_{sf}/α-Al_2O_3 composites.

(2) The hardness of C_{nt}/α-Al_2O_3 and C_{nt}-C_{sf}/α-Al_2O_3 composites is closely related to their relative density. The hardness and compactness of C_{nt}/α-Al_2O_3 and C_{nt}-C_{sf}/α-Al_2O_3 composites slightly decrease as the CNTs content increases.

(3) Flexural strength and fracture toughness of C_{nt}0.6 are 350 MPa and 6.3 MPa/m^2, which are 115% and 80% higher than that of C_{nt}0, respectively. Flexural strength and fracture toughness of C_{sf}5-nt06 composite are 465 MPa and 7.08 MPa/m^2, which are 37% and 13% higher than that of C_{nt}0.6, and 42% and 34% higher than that of C_{sf}5, respectively.

(4) Synchronously introducing C_{sf} and CNTs into α-Al_2O_3 matrix results in a bimodal grain size microstructure of C_{nt}-C_{sf}/α-Al_2O_3 composites, which accounts for the unique fractograph and the enhanced toughness of C_{nt}-C_f/α-Al_2O_3 composites.

Acknowledgment

This work was supported by the National Natural Science Foundation of China (no. 51461029) and Gansu Province science and technology major projects (no. 1602GKDD012).

References

[1] P.G. He, D.C. Jia, Y.T. Li, S. Yan, J.K. Yuan, X.M. Duan, Z.H. Yang, Y. Zhou, Preparation and mechanical performance of ductile C_{sf}/Al_2O_3–BN composites—Part 2: effects of fiber contents and ablation properties, Ceram. Int. 42 (2016) 11063–11069.
[2] Z.L. Li, J. Zhao, J.L. Sun, F. Gong, X. Ni, Reinforcement of Al_2O_3/TiC ceramic tool material by multi-layer graphene, Ceram. Int. 43 (2017) 11421–11427.
[3] O.S. Asiq Rahman, M. Sribalaji, B. Mukherjee, T. Laha, A.K. Keshr, Synergistic effect of hybrid carbon nanotube and graphene nanoplatelets reinforcement on processing, microstructure, interfacial stress and mechanical properties of Al_2O_3 nanocomposites, Ceram. Int. 44 (2018) 2109–2122.
[4] P.G. He, D.C. Jia, Y.T. Li, J.K. Yuan, S. Yan, Z.H. Yang, X.M. Duan, Y. Zhou, Preparation and mechanical performance of ductile C_{sf}/Al_2O_3–BN composites, Part 1: effects of fiber length and sintering temperature, Ceram. Int. 42 (2016) 9821–9829.
[5] https://doi.org/10.1016/j.ceramint.2017.05.138.
[6] Ba Nghiep Nguyen, Charles H. Henager Jr., Mode I fracture toughness prediction for multiwalled-carbon-nanotube reinforced ceramics, Eng. Fract. Mech. 147 (2015) 83–99.
[7] H.H. Zhang, Y.M. Zhang, B. Wang, J.F. Yang, Preparation and characterization of continuous alumina based fiber reinforced with orientated mullite whisker, J. Chem. Eng. 268 (2015) 109–115.
[8] Y.M. Zhang, Y.L. Zhang, J.C. Han, L.Y. Hu, The effect of sintering additive on fracture behavior of carbon-whisker-reinforced silicon carbide composites, Mater. Sci. Eng. A 480 (2008) 62–67.
[9] J. Echeberria, J. Ollo, M.H. Bocanegra-Bernal, A. Garcia-Reyes, C. Domínguez-Rios, A. Aguilar-Elguezabal, A. Reyes-Rojas, Sinter and hot isostatic pressing (HIP) of multi-wall carbon nanotubes (MWCNTs) reinforced ZTA nanocomposite: microstructure and fracture toughness, Int. J. Refract. Metals Hard Mater. 28 (2010) 399–406.
[10] Mehdi Estili, Sakka Yoshio, Recent advances in understanding the reinforcing ability and mechanism of carbon nanotubes in ceramic matrix composites, Sci. Technol. Adv. Mater. 15 (25pp) (2014) 064902.
[11] H. Ghobadi, A. Nemati, T. Ebadzadeh, Z. Sadeghian, H. Barzegar-Bafrooei, Improving CNT distribution and mechanical properties of MWCNT reinforced alumina matrix, Mater. Sci. Eng. A 617 (2014) 110–114.
[12] M.H. Bocanegra-Bernal, C. Dominguez-Rios, J. Echeberria, A. Reyes-Rojas, A. Garcia-Reyes, A. Aguilar-Elguezabal, Spark plasma sintering of multi-, single/double- and single-walled carbon nanotube-reinforced alumina composites: is it justifiable the effort to reinforce them? Ceram. Int. 42 (2016) 2054–2062.
[13] J.G. Jia, D.Q. Liu, C.Q. Gao, G.S. Ji, T.M. Guo, Preparation and mechanical properties of short carbon fibers reinforced α-Al_2O_3-based composites, Ceram. Int. 44 (2018) 19345–19351.
[14] Soumya Sarkar, Kr Probal, Das, Microstructure and physicomechanical properties of pressureless sintered multiwalled carbon nanotube/alumina nanocomposites, Ceram. Int. 38 (2012) 423–432.
[15] B. Mukherjee, O.S. A. R, A. Islam, M. S, A.K. Keshri, Plasma sprayed carbon nanotube and graphene nanoplatelets reinforced alumina hybrid composite coating with outstanding toughness, J. All. Comp. 727 (2017) 658–670.
[16] F.W. Zok, Developments in oxide fiber composites, J. Am. Ceram. Soc. 89 (11) (2006) 3309–3324.
[17] P.O. Guglielmi, D. Blaese, M.P. Hablitzel, G.F. Nunes, V.R. Lauth, D. Hotza, H.A. Al-Qureshi, R. Janssen, Microstructure and flexural properties of multilayered fiber-reinforced oxide composites fabricated by a novel lamination route, Ceram. Int. 41 (6) (2015) 7836–7846.
[18] E. Stoll, P. Mahr, H.G. Krüger, H. Kern, B.J.C. Thomas, A.R. Boccaccini, Fabrication technologies for oxide-oxide ceramic matrix composites based on electrophoretic deposition, J. Eur. Ceram. Soc. 26 (9) (2006) 1567–1576.
[19] T. Wei, Z.J. Fan, G.H. Luo, F. Wei, D.Q. Zhao, J.P. Fan, The effect of carbon nanotubes microstructures on reinforcing properties of SWNTs/alumina composite, Mater. Res. Bull. 43 (2008) 2806–2809.
[20] T. Bai, T.T. Xie, Fabrication and mechanical properties of WC-Al_2O_3 cemented carbide reinforced by CNTs, Mater. Chem. Phys. 201 (2017) 113–119.
[21] Z. Xia, L. Riester, W.A. Curtin, H. Lia, B.W. Sheldon, J. Liang, B. Chang, J.M. Xu, Direct observation of toughening mechanisms in carbon nanotube ceramic matrix composites, Act. Mater. 52 (2004) 931–944.
[22] P.O. Guglielmia, D. Blaesea, M.P. Hablitzelb, G.F. Nunesb, V.R. Lauth,

Microstructure and flexural properties of multilayered fiber-reinforced oxide composites fabricated by a novel lamination route, Ceram. Int. 41 (2015) 7836–7846.
[23] T. Shi, X.Z. Guo, H. Yang, Preparation and characterization of transparent boehmite (γ-AlOOH) Sol, J. Rare. Metal. Mater. Eng. 37 (2008) 73–75.
[24] J.J. Sha, J. Li, S.H. Wang, Y.C. Wang, Z.F. Zhang, J.X. Dai, Toughening effect of short carbon fibers in the ZrB_2–$ZrSi_2$ ceramic composites, Mater. Des. 75 (2015) 160–165.
[25] T. Bai, T.T. Xie, Fabrication and mechanical properties of WC-Al_2O_3 cemented carbide reinforced by CNTs, Mater. Chem. Phy. 201 (2017) 113–119.
[26] N. Bakhsh, F. Ahmad Khalid, A. Saeed Hakeem, Synthesis and characterization of pressureless sintered carbon nanotube reinforced alumina nanocomposites, Mater. Sci. Eng. A 578 (2013) 422–429.
[27] Shi C. Zhang, William G. Fahrenholtz, Greg E. Hilmas, Edward J. Yadlowsky, Pressureless sintering of carbon nanotube–Al_2O_3 composites, J. Eur. Ceram. Soc. 30 (2010) 1373–1380.
[28] M.N. Rahaman, Ceramic Processing and Sintering, CRC, New York, 2003.
[29] Yujie Fu, Ping Shen, Zhijie Hu, et al., The role of CuO–TiO_2 additives in the preparation of highstrength porous alumina scaffolds using directional freeze casting, Porous. Mater. 23 (2016) 539–547.
[30] M.A. Meyers, K.K. Chawla, Mechanical Behavior of Materials, CUP, New York, 2009.
[31] R.W. Rice, Mechanical Properties of Ceramics and Composites: Grain and Particle Effects, CRC Press, New York, 2000.